J. Fluid Mech. (2004), *vol.* 509, *pp.* 281–304.
DOI: 10.1017/S0022112004009395 Printed in the United Kingdom

Vortex motion in a weak background shear flow

By KONRAD BAJER[1], ANDREW P. BASSOM[2] AND ANDREW D. GILBERT[2]

[1]Institute of Geophysics, Warsaw University, Poland

[2]Department of Mathematical Sciences, University of Exeter, North Park Road, Exeter, Devon EX4 4QE, UK

(Received 27 October 2003 and in revised form 5 March 2004)

A point vortex is introduced into a weak background vorticity gradient at finite Reynolds number. As the vortex spreads viscously so the background vorticity becomes wrapped around it, leading to enhanced diffusion of vorticity, but also giving a feedback on the vortex and causing it to move. This is investigated in the linear approximation, using a similarity solution for the advection of weak vorticity around the vortex, at finite and infinite Reynolds number. A logarithmic divergence in the far field requires the introduction of an outer length scale L and asymptotic matching. In this way results are obtained for the motion of a vortex in a weak vorticity field modulated on the large scale L and these are confirmed by means of numerical simulations.

1. Introduction

The effect of a two-dimensional vortex on the distribution of a passive scalar in the plane is well known. The flow field of the vortex wraps up the passive scalar to form a spiral structure, leading to the diffusive decay of scalar fluctuations in the vicinity of the vortex. Several time scales are involved: in particular there is an enhanced shear–diffusion time scale for the destruction of scalar fluctuations on given closed streamlines (Moffatt & Kamkar 1983; Rhines & Young 1983; Bajer, Bassom & Gilbert 2001). The spiral distribution of the passive scalar also has a fractal nature, with a non-trivial box-counting dimension which can determine spectral power laws and anomalous diffusion properties (for example, Gilbert 1988; Vassilicos 1995).

When the passive scalar is replaced by weak vorticity new effects can come into play owing to the coupling of the vorticity to the flow field. Such vorticity might be present through perturbations to a vortex, for example if a vortex is immersed in weak ambient strain generated by other vortices, by vortex interactions, or by a vortex moving in a background of weak, filamented vorticity. These situations can occur in two-dimensional turbulence (for example Fornberg 1977; McWilliams 1984; Brachet *et al.* 1988; Dritschel 1989) but also have wider applicability to the modelling of vortices in general geophysical fluid flows (for example, Rhines & Young 1982; McCalpin 1987; Smith & Montgomery 1995; Brunet & Montgomery 2002; Montgomery & Brunet 2002).

Weak vorticity, much like a passive scalar, is subject to spiral wind-up and enhanced diffusion in the dominant axisymmetric flow field of a vortex (Lundgren 1982; Sutyrin 1989; Bernoff & Lingevitch 1994; Bassom & Gilbert 1998). However, vorticity is coupled into the flow field, and so can interact with the dynamics of the vortex. Interesting effects arise when it is coupled to a normal mode of the vortex, for such a mode can be stabilized or destabilized by the presence of weak vorticity in a critical

layer (Briggs, Daugherty & Levy 1970; Le Dizès 2000; Balmforth, Llewellyn Smith & Young 2001; Hall, Bassom & Gilbert 2003*a*, *b*). The resulting combination of normal mode and spiral wind-up of vorticity in a critical layer forms a 'quasi-mode' that is responsible for the 'rebound' phenomenon of suppression of non-axisymmetric vorticity fluctuations in perturbed Gaussian vortices, discussed by Bassom & Gilbert (1998, 1999, 2000) and Macaskill, Bassom & Gilbert (2002). There is an important analogy between the equations for inviscid planar fluid flow and magnetized electron plasmas (Briggs *et al.* 1970) which allows experimental verification of many of these results at very high Reynolds numbers (Schecter *et al.* 2000). A related area of study for fluid and analogous plasma systems is shear flow; see, for example, Balmforth, del Castillo Negrete & Young (1997).

Another effect of weak vorticity is to cause the vortex to move in the plane. This can be considered as a coupling to a mode with angular wavenumber $n = 1$, and this mode includes infinitesimal translations of the vortex (Smith & Rosenbluth 1990; Ting & Klein 1991; Lingevitch & Bernoff 1995; Llewellyn Smith 1995). In this paper we consider flows confined to the plane, and the case where the coherent vortex is immersed in a weak background gradient of vorticity; an example is that of a point vortex introduced at the midline of a weak plane Poiseuille shear flow. At one level the background vorticity field behaves like a passive scalar, being wrapped around by the coherent vortex and subject to enhanced diffusion processes. However, the weak background vorticity is coupled back to the flow field, and this feedback can set the vortex in motion. We will analyse this feedback within the linear approximation, for finite and infinite Reynolds number. Our work complements recent studies of Schecter & Dubin (1999, 2001) who consider the same problem, but rather in the limit of strong background vorticity and an infinite Reynolds number. Our results are qualitatively in agreement with theirs, but the analytical formulae obtained are different, pertaining to the opposite limit of a weak background flow.

Closely related to these studies is the problem in geophysical fluid dynamics of vortex motion on a beta-plane, for example modelling hurricane and cyclone motion. In the presence of a background gradient of planetary vorticity (modelled by the beta-effect), the motion generated by a vortex rearranges absolute vorticity, leading to a dipolar distribution of relative vorticity (a pair of 'beta gyres') which then sets the vortex in motion (for example, Reznik & Dewar 1994; Llewellyn Smith 1997; Sutyrin & Morel 1997). This mechanism is closely related to the one we study; in particular Llewellyn Smith (1997) confronts many of the issues we will face, and we will make frequent reference to this paper (which will be abbreviated to LS97) and its results, as we proceed. Appendix A gives a detailed comparison between the two papers. To summarize: the near field of the two problems is the same, but the far fields are different. In LS97, the far field supports Rossby waves; in our case instead the background flow is modulated on a large scale. In Schecter & Dubin (2001) the advection of vorticity by the background flow becomes important in the far field. These three different physical pictures for the far field yield similar formulae for the vortex motion. We also note that LS97 works in an inviscid framework, for an arbitrary initial vortex profile, whereas we include the effects of viscosity with a diffusing, Gaussian vortex. This enables us to quantify the effects of viscosity on the vortex motion and on the spatial structure of the vorticity field.

The flow geometry and basic mechanism leading to vortex motion are shown in figure 1 (see e.g. Cushman-Roisin 1994 for similar figures relating to motion on a beta-plane). We begin with a weak Poiseuille flow $\boldsymbol{U}_{\mathrm{b}} = \mu x^2 \hat{\boldsymbol{y}}$, depicted in figure 1(*a*). Here fluid at the origin (in the centre of the picture) is at rest, and there is a

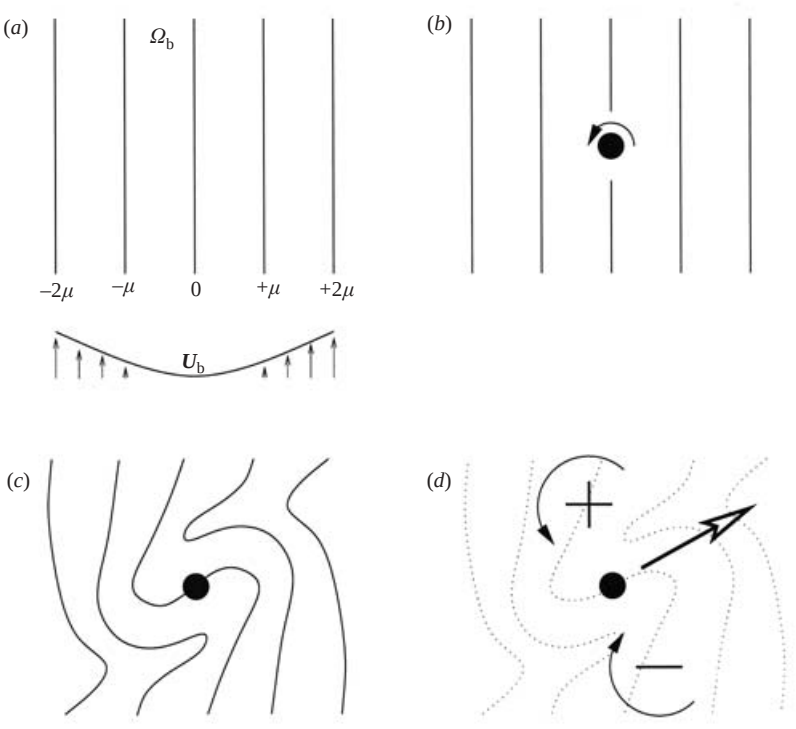

FIGURE 1. Basic mechanism for vortex motion. (*a*) A background vorticity gradient, (*b*) in which a vortex is introduced at $t=0$. (*c*) The distorted contours of the gradient give a flow field (*d*) which causes the vortex to move.

background vorticity gradient with $\Omega_b = 2\mu x$. At $t=0$ we introduce a point vortex at the origin (figure 1*b*), which has the effect of wrapping the background vorticity around it (figure 1*c*). This gives increased Ω_b on the upper, $+y$-side of the vortex, and decreased Ω_b on the lower, $-y$-side. This dipolar distribution of vorticity generates a flow field (figure 1*d*) which itself tends to set the vortex in motion to the right. This is the mechanism we study in this paper, in the linear approximation of a weak background field. Similar motion was found by Schecter & Dubin (2001) for their case of strong background shear, and they give additional physical arguments based on conservation laws to show that a vortex is attracted to regions of like-signed vorticity.

We note at the outset that the distortion of the background will be proportional to t for short times, giving a feedback of a vortex velocity of order μt, which on integrating suggests that the vortex displacement will be proportional to μt^2. Unfortunately, not only is this simple argument unable to predict the direction of motion of the vortex, but it turns out to be only partially correct, as the problem of vortex motion in a spatially infinite vorticity gradient set out above is actually ill-posed. It is necessary to introduce a new, long length scale L which cuts off the gradient, and this gives rise to an additional correction, which is logarithmic in t, to the μt^2 behaviour given above. Physically, the motion of the vortex is not a local problem, but depends on the far field of the vorticity distribution. This issue of regularizing a logarithmic divergence is also found in the study LS97 of a vortex on a beta-plane, but in that case it may be treated by matching to Rossby wave radiation in the far field.

The remainder of the paper is organized as follows. In § 2 the governing equations are set out and the problem specified, while § 3 presents some numerical results illustrating the phenomenon under discussion. We then develop in §§ 4–6 a similarity solution for a vortex in a spatially infinite gradient of vorticity, which builds on work by Pearson & Abernathy (1984), Moore (1985, hereafter referred to as M85) and Bajer (1998) for the evolution of a passive scalar gradient in the flow of a diffusing vortex. However, as alluded to above, there is a problem in fixing the far-field stream function, with a growing logarithmic term. To handle this, in § 7 we suppose that the vorticity gradient is modulated on a large scale L and by matching deduce results for the vortex motion. Section 8 considers the particular case of vortex motion at infinite Reynolds number, while the concluding § 9 offers detailed comparison between numerical and analytical results, and some final discussion.

2. Governing equations

The starting point is the equations for two-dimensional planar fluid motion, written in standard form as

$$\partial_t \Omega + J(\Omega, \Psi) = \nu \nabla^2 \Omega + G_\mathrm{b}, \qquad \Omega = -\nabla^2 \Psi, \tag{2.1}$$

with corresponding fluid flow $\boldsymbol{U} = (\partial_y \Psi, -\partial_x \Psi)$. Suppose we begin with a given background flow, which is a steady fluid motion maintained by some external body force G_b. In other words we specify $(\Omega_\mathrm{b}(\boldsymbol{r}), \Psi_\mathrm{b}(\boldsymbol{r}), G_\mathrm{b}(\boldsymbol{r}))$ to satisfy (2.1),

$$J(\Omega_\mathrm{b}, \Psi_\mathrm{b}) = \nu \nabla^2 \Omega_\mathrm{b} + G_\mathrm{b}, \qquad \Omega_\mathrm{b} = -\nabla^2 \Psi_\mathrm{b}. \tag{2.2}$$

Now a point vortex of circulation Γ is introduced at time $t = 0$ and we ask how both it and the background flow evolve. That is, $\Omega(\boldsymbol{r}, t)$ and $\Psi(\boldsymbol{r}, t)$ are sought that solve (2.1) with the given background $G_\mathrm{b}(\boldsymbol{r})$ and satisfy the initial condition

$$\Omega(\boldsymbol{r}, 0) = \Omega_\mathrm{b}(\boldsymbol{r}) + \Omega_\mathrm{v}(\boldsymbol{r}, 0), \qquad \Omega_\mathrm{v}(\boldsymbol{r}, 0) \equiv \Gamma \delta(x)\delta(y) \tag{2.3}$$

and the far-field constraint

$$\Psi(\boldsymbol{r}, t) = \Psi_\mathrm{b}(\boldsymbol{r}) + (\Gamma/2\pi) \log r + O(r^{-1}) \qquad (r \to \infty), \tag{2.4}$$

with $r \equiv |\boldsymbol{r}|$. This latter condition is designed to rule out possible flows, for example a uniform flow, imposed at infinity. If there were no background flow, so that $(\Omega_\mathrm{b}, \Psi_\mathrm{b}, G_\mathrm{b}) \equiv 0$, the vortex introduced at $t = 0$ simply spreads diffusively as a Gaussian or Lamb vortex,

$$\Omega_\mathrm{v}(\boldsymbol{r}, t) = \frac{\Gamma}{4\pi\nu t} \exp(-r^2/4\nu t) \tag{2.5}$$

and, given the dimensions $[\Gamma] = [\nu] = \mathscr{L}^2/\mathscr{T}$, we may define a Reynolds number R based on the vortex, $R \equiv \Gamma/2\pi\nu$.

We now turn to the background flow. We shall concentrate on two; the first is standard plane Poiseuille flow, with

$$\Omega_\mathrm{b}(\boldsymbol{r}) = 2\mu x, \qquad \Psi_\mathrm{b}(\boldsymbol{r}) = -\tfrac{1}{3}\mu x^3, \qquad \boldsymbol{U}_\mathrm{b}(\boldsymbol{r}) = \mu x^2 \, \hat{\boldsymbol{y}}, \qquad G_\mathrm{b} = 0. \tag{2.6}$$

Given the parameters Γ, ν and μ defined so far, there is no dimensionless measure of μ, which has the dimensions $[\mu] = 1/\mathscr{L}\mathscr{T}$. Instead we introduce a length scale $L_\mathrm{vb} = (\Gamma/\mu)^{1/3}$ at which the flow of a point vortex of strength Γ and the background (2.6) have a similar magnitude. When the two flows are combined, inside this radius the flow will be recirculating, dominated by the vortex, and outside it is approximately unidirectional and dominated by the background.

The second background flow we consider has a bounded vorticity distribution, which is convenient both numerically and analytically. It takes the form

$$\Omega_{\rm b} = 2\mu L \sin(x/L), \qquad \Psi_{\rm b} = 2\mu L^2(L\sin(x/L) - x), \tag{2.7a}$$

$$\boldsymbol{U}_{\rm b} = 2\mu L^2[1-\cos(x/L)]\,\hat{\boldsymbol{y}}, \qquad G_{\rm b} = \nu L^{-2}\Omega_{\rm b} \tag{2.7b}$$

and is periodic with period $2\pi L$. On scales $x/L \ll 1$ this sinusoidal flow reduces approximately to the Poiseuille flow (2.6). Notice that a passive particle placed initially at the origin will remain at rest; not so a vortex, which should move by the mechanism shown in figure 1. At this juncture it is worth remarking on the role of the background forcing $G_{\rm b}$. This has been introduced in order to state the problem of vortex motion cleanly for any Reynolds number R and any background flow. The forcing term plays no role in the subsequent analytical development, and if the background flow is inviscid and a two-dimensional Euler flow, then in any case $G_{\rm b} = 0$.

The problem of vortex motion in the sinusoidal flow (2.7) is specified by the dimensionless parameters R and $L/L_{\rm vb}$. Our subsequent analytical study will be valid under the conditions

$$R \equiv \Gamma/2\pi\nu \geqslant O(1), \tag{2.8a}$$

$$L \ll L_{\rm vb} \equiv (\Gamma/\mu)^{1/3}, \tag{2.8b}$$

$$t \ll L^2/\Gamma. \tag{2.8c}$$

These three requirements, which will be used frequently in what follows, admit straightforward interpretation. The first is a statement that the vortex is of moderate or high Reynolds number, while the second stipulates that on scales of order L about the vortex the flow is dominated by the vortex itself. In this event it is then legitimate to linearize the evolution of the background vorticity about a strong vortex; the contrasting situation when $L \gg L_{\rm vb}$ was examined by Schecter & Dubin (2001) for $R = \infty$. We remark that $L_{\rm vb}$ may be identified with a Rhines (1975) scale as discussed in Appendix A. The final constraint (2.8*c*) concerns the duration of the validity of our results. The presence of the vortex (which has angular velocity $\alpha \simeq \Gamma/2\pi r^2$ for large r) means that the background vorticity rotates through angles of order unity in a time of order L^2/Γ. At times later than this the background cannot justifiably be thought of as being fixed at large distances, since the vortex shreds vorticity even on a scale L.

3. Numerical simulation of vortex motion

In this section we present some numerical simulations that show the phenomenon depicted in figure 1, before we become involved in detailed analysis. The vorticity equation (2.1) is solved numerically in the periodic domain $(x, y) \in [-\pi, \pi]^2$ with initial condition (2.3) and the background flow (2.7). Rather than formally non-dimensionalizing, it is more convenient to prescribe the length $L = 1$, circulation $\Gamma = 2\pi$, and vary the parameters μ and ν. Our code uses periodic boundary conditions whereas in our later analysis we shall study a single vortex in the infinite plane; the effects of this difference will be revisited in § 9. Finally, note that the flow used has a steady flux $\langle \boldsymbol{U}_{\rm b}\rangle = 2\mu L^2\hat{\boldsymbol{y}}$ in (2.7); this generates a secular term in $\Psi_{\rm b}$ which requires separate handling in the code that steps (2.1) forward in time.

Figure 2 shows a simulation at a resolution 512^2, with the parameters $\nu = 0.001$ and $\mu = 0.75$ for various times between $t = 0$ and $t = 2$. The corresponding dimensionless

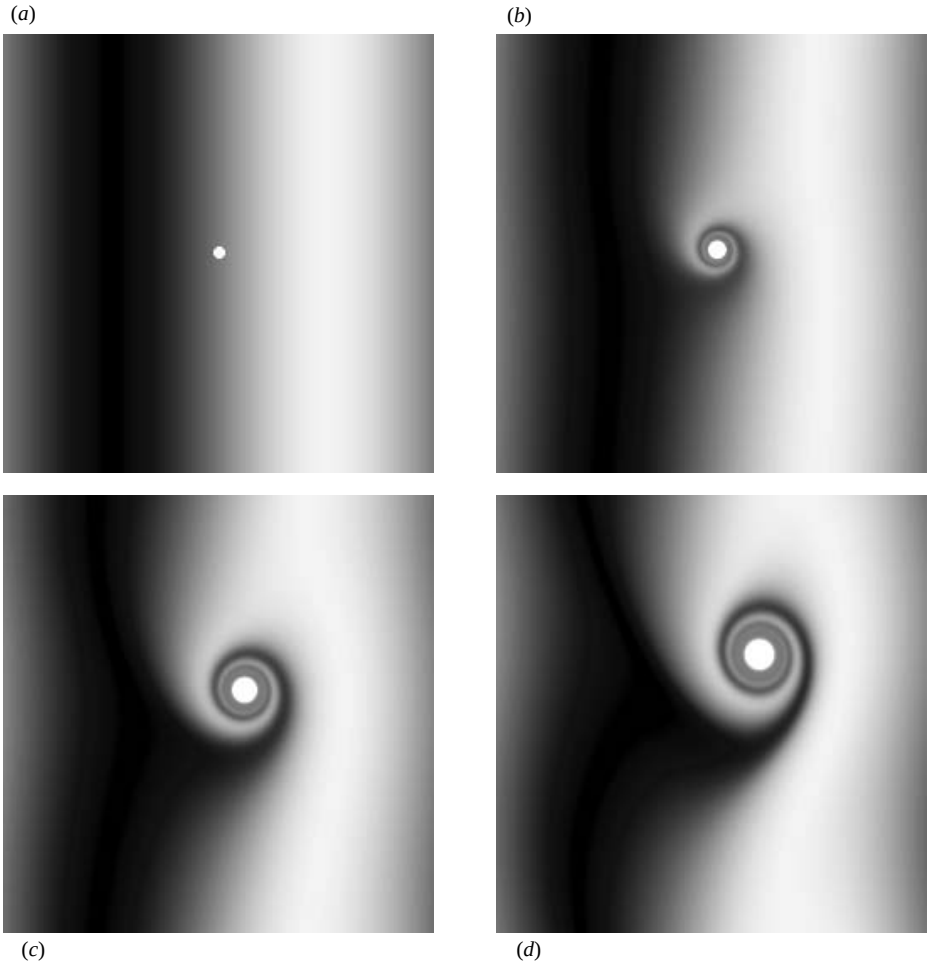

FIGURE 2. The panels illustrate vortex motion for $\nu = 0.001$, $\Gamma = 2\pi$, $\mu = 0.75$, $L = 1$ and (*a*) $t = 0$, (*b*) 0.4, (*c*) 1.2 and (*d*) 2.0. Shown is $\omega_{\rm cut}(x, y, t)$ defined in (3.2).

parameters are

$$R = 1000, \quad L/L_{\rm vb} \simeq 0.5, \quad \Gamma t/L^2 \leqslant 4\pi \tag{3.1}$$

and so we are effectively in the inviscid limit of large R. The vortex in figure 2 is strong compared with the background vorticity and so the vorticity field is cut off at $+2\mu$ to make the background visible; plotted is

$$\omega_{\rm cut}(x, y, t) = \min(\omega(x, y, t), 2\mu) \tag{3.2}$$

on a grey scale from -2μ (black) to $+2\mu$ (white). The vortex then appears as a white disk (of exaggerated size). Rather than attempting to impose the strict form of (2.3), the initial condition adopted in practice was $\omega(x, y, 0^+) = (\Gamma/4\pi r_0^2)\,{\rm e}^{-r^2/4r_0^2}$ with $r_0 = 0.015$; tests showed that the value of r_0 chosen made little difference to our results.

In figure 2 we clearly see the wind-up of the background vorticity about the vortex (white disk) which is coupled to the resulting vortex motion, in the $+x$- and $+y$-directions, as also seen by Schecter & Dubin (2001). Note that one feature that develops in the background vorticity distribution is a 'hole' around the vortex, where

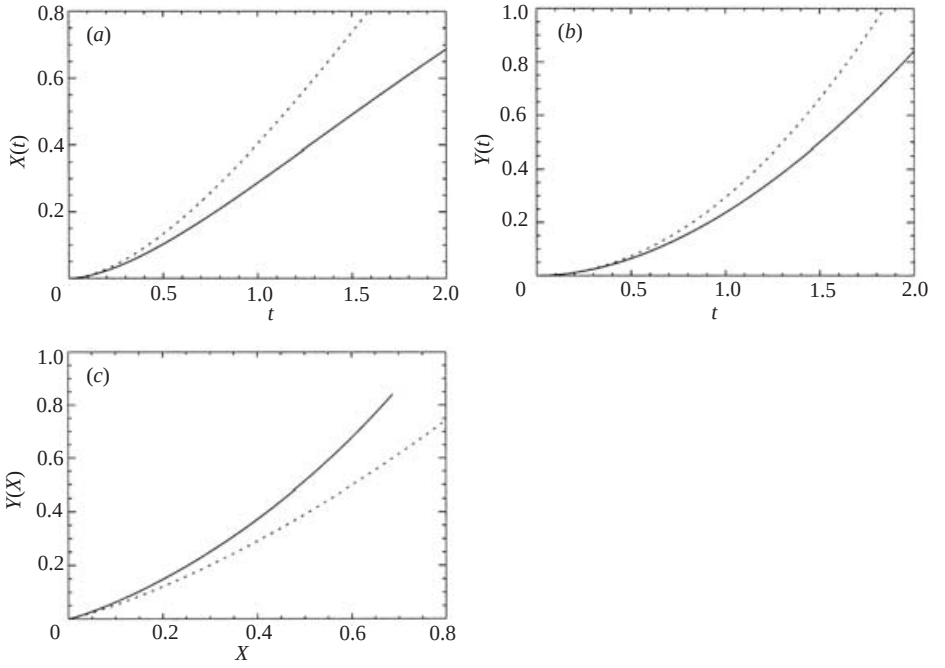

FIGURE 3. Plotted are (*a*) $X(t)$, (*b*) $Y(t)$ and (*c*) $Y(X)$ for the motion of the vortex centre shown graphically in figure 2. Shown are numerical results (solid) and asymptotic theory (3.3) for large R (dotted).

the background vorticity has been destroyed through the shear–diffuse mechanism. The hole appears as a grey annulus (corresponding to $\omega = 0$) about the white disk of the vortex, and inside the spirally wrapped background. The hole is also a feature of the analogous passive scalar problem (M85; Bajer 1998), and is important for studying the inviscid limit in § 8 below. The vorticity hole is characterized by two scales; the first is its overall radius $O(\sqrt{\nu t})$, which may be defined as the distance at which vorticity is carried through angles of order unity by the central vortex. The second is the radius at which viscosity damps the vorticity to exponentially small values, which from equation (4.1) of M85 is $O(R^{1/3}\sqrt{\nu t})$ (see also Bajer 1998). In this situation of large Reynolds number the vortex is wholly contained within the hole and can in fact be considered as a point vortex in the given weak background vorticity field.

We suppose that the centre of the vortex is located at $(X(t), Y(t))$, which is determined by following the position of maximum vorticity in the simulations. Figure 3 shows the motion of the vortex; here solid lines denote the measured forms of $X(t)$ (*a*), $Y(t)$ (*b*) and $Y(X)$ (*c*). The theory we develop below under the assumptions (2.8*a–c*) gives the approximate formula

$$X(t) + \mathrm{i}Y(t) = -(\Gamma/4\pi)\mu t^2 \left[\tfrac{1}{2}\log(\Gamma t/8\pi L^2) - \tfrac{5}{4} + \tfrac{3}{2}\gamma - \tfrac{1}{4}\right], \tag{3.3}$$

where $\gamma \simeq 0.577216$ is Euler's constant. This result is valid for large R and is independent of R. The motion depends not only on the local gradient μ, but also on the scale L of the background vorticity. Figure 3 shows fair agreement between this approximate solution (dotted) and the numerical results (solid); a more detailed comparison will be made in § 9 below, after the theory itself has been developed.

Note that we have taken μ fairly large in our simulation with $L/L_{\rm vb} \simeq 0.5$, which is not very small in view of (2.8*b*). However, there is an element of compromise involved in the selection of μ. At smaller values than that used here the theory holds well, but the motion of the vortex is smaller, which makes it less easily studied numerically and less striking graphically. On the other hand, at larger $\mu \geqslant 1$ the theory begins to break down, unsurprisingly. At this stage though, the important information conveyed by figure 2 is that the mechanism sketched in figure 1 is operative, and we now consider the effect analytically.

4. The linearized problem and translation modes

Given a steady background flow $(\Omega_{\rm b}, \Psi_{\rm b}, G_{\rm b})$, the full nonlinear problem is to solve the vorticity equation (2.1) with the initial condition (2.3) and far-field behaviour (2.4). Some means of diagnosing the resulting vortex motion is also necessary. Generally this all has to be done numerically; however analytical progress is possible on linearizing (2.1) about the diffusing Gaussian vortex (2.5), setting

$$\Omega(\boldsymbol{r}, t) = \Omega_{\rm v}(\boldsymbol{r}, t) + \omega(\boldsymbol{r}, t) + \cdots, \quad \Psi(\boldsymbol{r}, t) = \Psi_{\rm v}(\boldsymbol{r}, t) + \psi(\boldsymbol{r}, t) + \cdots \tag{4.1}$$

and thereby obtaining the linearized vorticity equation,

$$\partial_t \omega + \alpha \partial_\theta \omega + \beta \partial_\theta \psi = \nu \nabla^2 \omega + G_{\rm b}, \qquad \omega = -\nabla^2 \psi. \tag{4.2}$$

Here the functions α and β characterize the diffusing vortex structure according to

$$\alpha(r, t) \equiv -r^{-1} \partial_r \Psi_{\rm v} = \frac{\Gamma}{2\pi r^2} \left(1 - {\rm e}^{-r^2/4\nu t}\right), \tag{4.3a}$$

$$\beta(r, t) \equiv r^{-1} \partial_r \Omega_{\rm v} = -\frac{\Gamma}{8\pi \nu^2 t^2} \, {\rm e}^{-r^2/4\nu t}. \tag{4.3b}$$

We then solve (4.2) subject to initial and far-field conditions that follow from (2.3) and (2.4),

$$\omega(\boldsymbol{r}, t) \to \Omega_{\rm b}(\boldsymbol{r}) \qquad (t \to 0^+), \tag{4.4a}$$

$$\psi(\boldsymbol{r}, t) = \Psi_{\rm b}(\boldsymbol{r}) + O(r^{-1}) \qquad (r \to \infty). \tag{4.4b}$$

Convergence in (4.4*a*) is obviously non-uniform at the location $r = 0$ of the initial point vortex as $t \to 0^+$.

Naturally, the linearized system (4.2) is only an approximation and, for the case of a background Poiseuille flow (2.6), it is valid provided $r \ll L_{\rm vb}$. For the sinusoidal background flow (2.7) the linearization is valid on scales up to and including $r = O(L)$, given that (2.8*b*) holds.

The linear system (4.2) can be broken into harmonics in θ and we may set

$$\omega = \sum_n \omega_n(r, t) {\rm e}^{{\rm i}n\theta}, \quad \psi = \sum_n \psi_n(r, t) {\rm e}^{{\rm i}n\theta}, \quad G_{\rm b} = \sum_n G_n(r) {\rm e}^{{\rm i}n\theta}, \tag{4.5}$$

with the usual conditions applied to ensure that these fields are real. Then we have that

$$\partial_t \omega_n + {\rm i}n\alpha\omega_n + {\rm i}n\beta\psi_n = \nu \Delta_n \omega_n + G_n, \qquad \omega_n = -\Delta_n \psi_n, \tag{4.6}$$

with $\Delta_n \equiv \partial_r^2 + r^{-1}\partial_r - r^{-2}n^2$.

To detect the motion of the vortex in the linear approximation we need to understand solutions of the vorticity equation corresponding to solid-body translation of the vortex (see LS97). If we consider the unforced ($G_{\rm b} = 0$) vorticity equation (2.1),

it admits the exact solution

$$\Omega = \Omega_{\rm v}(x - X(t), y - Y(t), t), \tag{4.7a}$$

$$\Psi = \Psi_{\rm v}(x - X(t), y - Y(t), t) + \dot{X}(t)y - \dot{Y}(t)x, \tag{4.7b}$$

which corresponds to a diffusing vortex (2.5) with centre $(X(t), Y(t))$ carried in a uniform flow $\boldsymbol{U} \sim (\dot{X}(t), \dot{Y}(t))$ imposed at infinity. Expanding for small (X, Y) yields an exact solution to the linearized problem (4.2) (with $G_{\rm b} = 0$),

$$\omega = -(Xx + Yy)\beta, \qquad \psi = (Xx + Yy)\alpha + \dot{X}y - \dot{Y}x \tag{4.8}$$

and hence we have an exact solution of (4.6) (with $G_1 = 0$) involving the $n = 1$ mode only. This form may be expressed compactly as

$$\omega_1 = \omega_{\rm trans} \equiv -\tfrac{1}{2}Z^*(t)r\beta(r, t), \qquad \psi_1 = \psi_{\rm trans} \equiv \tfrac{1}{2}Z^*(t)r\alpha(r, t) - \tfrac{1}{2}{\rm i}r\dot{Z}^*(t), \tag{4.9}$$

where the complex function $Z(t) \equiv X(t) + {\rm i}Y(t)$ has been introduced. We remark that the solution (4.9), which we label as $\mathscr{A}_{\rm trans}$, is valid for any $Z(t)$ and will be used to identify motion of the coherent vortex.

5. Similarity solution in a uniform background vorticity gradient

We start by considering the evolution of a vortex in the uniform background gradient (2.6). Mathematically, we therefore attempt to solve the linearized vorticity equation (4.2) with the fields matched through conditions (4.4*a*, *b*) to the underlying Poiseuille flow (2.6). We have previously noted that linearization is justified provided $r \ll L_{\rm vb}$, but we will find that we are unable to impose the far-field condition (4.4*b*) directly. However, our calculation will not have been in vain, for we shall discover that the solution obtained constitutes an inner solution to the problem of vortex motion in the sinusoidal background profile (2.7).

The Poiseuille flow (2.6) involves just the modes $n = 1$ (with $\omega_1 = \mu r$, $\psi_1 = -\frac{1}{8}\mu r^3$) and $n = 3$ (with $\omega_3 = 0$, $\psi_3 = -\frac{1}{24}\mu r^3$) together with their complex conjugates (see (4.5)). Also there is no forcing term, so $G_n \equiv 0$. The $n = 3$ component corresponds to an irrotational external flow, and while it will distort the vortex it has no implications for vortex motion within our linearized problem. We can therefore safely drop the mode $n = 3$ henceforth, and can concentrate on the $n = 1$ component. The problem is then to solve (4.6) with $n = 1$, that is

$$\partial_t\omega_1 + {\rm i}\alpha\omega_1 + {\rm i}\beta\psi_1 = \nu\Delta_1\omega_1, \qquad \omega_1 = -\Delta_1\psi_1, \tag{5.1}$$

subject to the matching conditions (4.4*a*, *b*)

$$\omega_1(r, t) \to \mu r \qquad (t \to 0^+), \tag{5.2a}$$

$$\psi_1(r, t) = -\tfrac{1}{8}\mu r^3 + O(r^{-1}) \qquad (r \to \infty). \tag{5.2b}$$

We approach this task using a similarity solution. While we have in mind $n = 1$, this particular solution is just one of a whole family, valid for any value n. We therefore retain a general value for n in this paragraph only, and set

$$\omega_n = \mu r^n\zeta(w), \qquad \psi_n = \mu r^n\nu t\chi(w), \qquad w = r/\sqrt{\nu t}. \tag{5.3}$$

Substituting into (4.6) (with $G_n \equiv 0$) gives the fourth-order system for $\chi(w)$, $\zeta(w)$

$$\zeta'' + \zeta'\left(\frac{2n+1}{w} + \frac{w}{2}\right) - \zeta\,\frac{{\rm i}nR}{w^2}\left(1 - {\rm e}^{-w^2/4}\right) + \chi\,\frac{{\rm i}nR}{4}\,{\rm e}^{-w^2/4} = 0, \tag{5.4a}$$

$$-\zeta = \chi'' + \frac{2n+1}{w}\,\chi'. \tag{5.4b}$$

In equation (5.4a) the first two terms represent evolution under the diffusion equation while the last two involve the angular velocity and coupling to the stream function respectively. If this coupling were dropped we would recover the passive scalar problem discussed by Pearson & Abernathy (1984), M85 and Bajer (1998).

With n again set firmly to unity, the matching conditions (5.2a,b) become

$$\zeta(w) \to 1 \qquad (w \to \infty), \tag{5.5a}$$

$$\chi(w) = -\tfrac{1}{8}w^2 + O(w^{-2}) \qquad (w \to \infty). \tag{5.5b}$$

The system (5.4a,b) has four linearly independent solutions, which we denote $\mathscr{A}_1$–$\mathscr{A}_4$. Frobenius expansions reveal that just two of these solutions, say $\mathscr{A}_1$ and $\mathscr{A}_2$, are finite at the origin and they expand in even powers of w. The first solution may be taken to be simply the translation mode, and, if $Z \equiv \mu\nu t^2$ in $\mathscr{A}_{\text{trans}}$ (4.9), we obtain this exact solution, $\mathscr{A}_1$,

$$\zeta = \tfrac{1}{8}R\,\mathrm{e}^{-w^2/4}, \quad \chi = \tfrac{1}{2}Rw^{-2}\left(1-\mathrm{e}^{-w^2/4}\right) - \mathrm{i}. \tag{5.6}$$

Notice how the values of ζ and χ at the origin are linked to the flow at infinity. The second regular solution $\mathscr{A}_2$ may be chosen so that $\chi(0)=0$, which corresponds to zero flow at the origin, and so no motion of the vortex. It can be expressed as a Frobenius expansion or computed numerically and, being a key ingredient in our calculations, we will return to it shortly.

Now we switch to the behaviour for large w, where the system (5.4a,b) reduces to

$$\zeta'' + \zeta'\left(3w^{-1} + \tfrac{1}{2}w\right) - \zeta\mathrm{i}Rw^{-2} \simeq 0, \qquad -\zeta = \chi'' + 3w^{-1}\chi'; \tag{5.7}$$

only terms that are exponentially small have been eliminated. This pair of equations partially decouples and one straightforward solution of this system is $\mathscr{B}_1$,

$$\zeta = 0, \quad \chi = 1, \tag{5.8}$$

corresponding to uniform flow at infinity. A second solution has the large-w expansions

$$\zeta = 1 - \mathrm{i}Rw^{-2} + O(w^{-4}), \tag{5.9a}$$

$$\chi = -\tfrac{1}{8}w^2 + \tfrac{1}{2}\mathrm{i}R\log w + O(w^{-2}\log w) \tag{5.9b}$$

and we call this solution $\mathscr{B}_2$. Notice that there is no constant term in (5.9b) and this has been arranged so that this solution is clearly distinguished from $\mathscr{B}_1$ in (5.8). The remaining two solutions are $\mathscr{B}_3$, with $\zeta=0$ and $\chi=w^{-2}$, and $\mathscr{B}_4$, for which both fields decay exponentially rapidly for large w. These latter two solutions will prove unimportant for us.

The general solution that is regular at the origin can be written schematically in two alternative ways, either as a sum of linear multiples of the $\mathscr{A}_i$ solutions or in terms of the far-field solutions,

$$(\chi,\zeta) = a_1\mathscr{A}_1 + a_2\mathscr{A}_2 = b_1\mathscr{B}_1 + b_2\mathscr{B}_2 + b_3\mathscr{B}_3 + b_4\mathscr{B}_4. \tag{5.10}$$

Looking at the far-field expression, we require $b_2=1$ from (5.5a) and the values of b_3 and b_4 are immaterial. The usual procedure would be to fix b_1 from (5.5b), implying the absence of an imposed flow at infinity. These two constants would then in principle determine the two unknown degrees of freedom a_1 and a_2; the former determines the translation of the vortex and so permits us to identify $Z(t)$ (see (5.6)). There is however a significant obstacle to this strategy. Once b_2 is fixed as unity, there is no means of selecting b_1, b_3 and b_4 in order to eliminate the growing logarithmic

term $\frac{1}{2}\mathrm{i}R\log w$ in χ in (5.9*b*). Such a logarithmic term is disallowed by the matching condition (5.5*b*) which, in physical variables, is designed to eliminate an additional uniform flow at infinity. This would correspond to a term $\psi \propto r$, or equivalently $\chi \propto 1$.

However, we have generated a term $\chi \propto \log w$ (or $\psi \propto r\nu t\log(r/\sqrt{\nu t})$), which corresponds to a spatially increasing (and time-dependent) flow. The upshot is that the linearized problem of a vortex in a spatially extended vorticity gradient must be ill-posed and the long-range motion driven by the vortex, in conjunction with an unbounded vorticity distribution, necessarily results in a logarithmically divergent flow. There are two sensible ways to proceed. We could adopt the methodology used by Schecter & Dubin (2001) and study the fully nonlinear problem but, rather, we shall assume the background vorticity field is modulated on a large length scale L, so that the linear approximation remains valid, and this will enable us to handle the logarithm properly by matched asymptotic expansions. We remark that similar logarithmic divergences appear in Schecter & Dubin (2001) and in the beta-plane study LS97; the relationship between the far fields in our study and these is discussed in Appendix A.

Before we do this, we briefly return to the solution $\mathscr{A}_2$. This is determined by imposing $\chi(0)=0$, which corresponds to fixing the vortex at the origin. Following the form of $\mathscr{A}_2$ outwards, it will evolve to some combination $\sum_{i=1}^{4} b_i\mathscr{B}_i$ for large w. It is convenient to normalize so that $b_2=1$, and thereby satisfy the condition (5.5*a*). We also let $b_1=RF(R)$, whereupon

$$\mathscr{A}_2 = RF(R)\mathscr{B}_1 + \mathscr{B}_2 + b_3\mathscr{B}_3 + b_4\mathscr{B}_4, \tag{5.11}$$

with the function $F(R)$ to be determined asymptotically or numerically; this is the subject of the next section. Under these conditions $\mathscr{A}_2$ has the far-field behaviour

$$\zeta = 1 - \mathrm{i}Rw^{-2} + O(w^{-4}), \tag{5.12a}$$

$$\chi = -\tfrac{1}{8}w^2 + \tfrac{1}{2}\mathrm{i}R\log w + RF(R) + O(w^{-2}\log w) \tag{5.12b}$$

and, physically, if we wish to fix the vortex at the origin, this is the flow that should be imposed at infinity. Notice that the most general solution to (5.4) and (5.5*a*) (but excluding (5.5*b*)) is then just $a_1\mathscr{A}_1 + \mathscr{A}_2$.

Finally we leave the similarity-variable framework. When rewritten in terms of $\omega_1(r,t)$ and $\psi_1(r,t)$ using (5.3) our similarity forms provide a solution to the corresponding problem in (r,t); that is (5.1) and (5.2*a*). However, a less restrictive solution can be obtained by replacing $a_1\mathscr{A}_1$ by a general translation mode in (4.9), of the form $\mathscr{A}_{\mathrm{trans}}$ for any $Z(t)$. This more general solution, which we can write schematically as $\mathscr{A}_{\mathrm{trans}} + \mathscr{A}_2$, solves (5.1) and (5.2*a*) (but not (5.2*b*)) and has the far-field behaviour

$$\omega_1 = \mu r - \mathrm{i}R\mu\nu t r^{-1} + \cdots, \tag{5.13a}$$

$$\psi_1 = -\tfrac{1}{8}\mu r^3 + R\mu\nu t r\left[\tfrac{1}{2}\mathrm{i}\log(r/\sqrt{\nu t}) + F(R)\right] - \tfrac{1}{2}\mathrm{i}r\dot{Z}^*(t) + \cdots. \tag{5.13b}$$

This is the far-field expansion of our inner problem and the additional flexibility of having an arbitrary $Z(t)$ will be essential when we come to match to an outer solution in § 7.

6. Evaluation of $F(R)$

In this section we calculate the function $F(R)$ in (5.12*b*) both numerically and asymptotically. To do this we isolate $\mathscr{A}_2$ numerically by solving the system (5.4)

R	$F(R)$ (asymptotic)	$F(R)$ (numerical)	$G(R)$ (numerical)
5	$0.393 - \mathrm{i}0.547$	$0.291 - \mathrm{i}0.519$	$-0.439 - \mathrm{i}0.581$
10	$0.393 - \mathrm{i}0.720$	$0.367 - \mathrm{i}0.706$	$-0.412 - \mathrm{i}0.733$
20	$0.393 - \mathrm{i}0.893$	$0.379 - \mathrm{i}0.895$	$-0.381 - \mathrm{i}0.758$
40	$0.393 - \mathrm{i}1.12$	$0.384 - \mathrm{i}1.067$	$-0.383 - \mathrm{i}0.768$

TABLE 1. Asymptotic (6.2) and numerical determinations of $F(R)$. Also given is the function $G(R)$ defined in (7.14).

subject to the boundary conditions

$$\chi(0) = 0, \quad \chi'(0) = \zeta'(0) = 0, \quad \zeta \to 1 \quad \text{as} \quad w \to \infty. \tag{6.1}$$

This was done using the NAG routine D02GBF on an interval $0 \leqslant w \leqslant w_{\max}$ with $w_{\max}$ as large as 400; the range has to be increased with R because the expansions for large w proceed in powers of Rw^{-2}. The two-term expansion given in (5.12*a*) was used as the boundary condition on ζ at $w_{\max}$ and $F(R)$ then extracted from the value of χ there; see (5.12*b*). Checks were made by using other codes to solve (5.4) subject to (6.1) but the procedure described turned out to be the most reliable for our purposes.

Results for $F(R)$ are given in table 1. For large R we will shortly establish the asymptotic approximation

$$F(R) \sim \tfrac{1}{8}(\pi - 2\mathrm{i}(\log R + \gamma)), \tag{6.2}$$

with γ again denoting Euler's constant. It is seen from the table that the asymptotic prediction (6.2) agrees very well with the computations for large R, and is even quite reasonable for moderate values as low as $R = 10$. In order to derive the large-R result (6.2) we build on the asymptotic study of M85, who considered the advection and diffusion of a passive scalar in a spreading Gaussian vortex (see also related work by Pearson & Abernathy 1984 and Bajer 1998). This problem amounts to solving (5.4*a*) (for $n = 1$) with the stream function coupling term,

$$\tfrac{1}{4}\chi \mathrm{i}R\, \mathrm{e}^{-w^2/4} \tag{6.3}$$

deleted, and ζ now plays the role of a passive scalar; the appropriate boundary conditions are $\zeta'(0) = 0$ and $\zeta(\infty) = 1$. M85 showed that in the formal limit $R \to \infty$ the solution is characterized by $\zeta \ll 1$ (exponentially small in R) for $w \ll R^{1/3}$; in this region the scalar has been homogenized by the vortex. The actual vortex, of scale $w = O(1)$, lies well inside this zone.

Now suppose we take this passive scalar solution for vorticity ζ, and reconstruct the corresponding stream function χ from (5.4*b*) with the boundary conditions $\chi(0) = \chi'(0) = 0$ (from (6.1)). This can be written in integral form

$$2\chi(w) = \int_0^w \left(\frac{s^3}{w^2} - s\right) \zeta(s)\, \mathrm{d}s, \tag{6.4}$$

which demonstrates that $\chi(w)$ is also exponentially small for $w \ll R^{1/3}$. The conclusion is that the awkward stream function coupling term (6.3) is actually small throughout

space so that the approximation which treats ζ as a passive scalar is correct, to exponential accuracy in $R \gg 1$.†

Motivated by this observation, we therefore use (6.4) to compute the leading far-field behaviour for χ using the complete asymptotic solution found in M85. The relevant part of his solution is simply

$$\zeta(w) \sim \exp(-\mathrm{i}R/w^2). \tag{6.5}$$

This is valid for $R^{1/4} \ll w = O(R^{1/2})$, gives the dominant contribution to the integral (6.4) and agrees with (5.12*a*). Once $w = O(R^{1/4})$ an alternative expression for ζ holds (see M85) but this region makes no contribution to (6.8) to the accuracy given.

Equation (6.5) may be obtained either from equations (2.2), (2.3), (4.1) of M85, or deduced from (5.4*a*) using the balance $\frac{1}{2}w\zeta' \sim \mathrm{i}Rw^{-2}\zeta$. Using results appearing in chapter 5 of Abramowitz & Stegun (1965), the integral in (6.4) may be expressed as

$$4\chi(w) = w^2(E_3(z) - E_2(z)) = w^2\left[-\tfrac{1}{2}(z+1)\mathrm{e}^{-z} + z(\tfrac{1}{2}z+1)E_1(z)\right], \tag{6.6}$$

where $z \equiv \mathrm{i}R/w^2$ and $E_n(z)$ denotes the exponential integral

$$E_n(z) = \int_1^\infty \frac{\mathrm{e}^{-zt}}{t^n}\,\mathrm{d}t \qquad (t = w^2/s^2). \tag{6.7}$$

We are interested in the far field $w \to \infty$ which corresponds to $z \to 0$. Applying the asymptotic series for $E_1(z)$ with z small leads to

$$\chi(w) = -\tfrac{1}{8}w^2 + \tfrac{1}{4}\mathrm{i}R\left(2\log w - \gamma - \log R - \tfrac{1}{2}\mathrm{i}\pi\right), \tag{6.8}$$

where γ is Euler's constant. This expression, valid for large R, is of the form of (5.12*b*), which holds for any R, and it is then an elementary task to deduce that the large-R form of $F(R)$ is precisely (6.2).

This result is derived for a uniform gradient, and so forms part of the inner solution, valid for $r \ll L$, of the full problem of vortex motion in a sinusoidal background vorticity distribution. As a check on the consistency of this, we note that the size of the hole in the vorticity distribution is $w = O(R^{1/2})$, which in terms of real variables is $r = O(\sqrt{R\nu t}) = O(\sqrt{\Gamma t}) \ll L$, from (2.8*c*). Within the restrictions we placed on our analysis the hole is always well within the outermost scale L.

7. Matching to the far field and vortex motion

We have developed the solution of a vortex in a uniform vorticity gradient (2.6) as far as we can. Next, suppose that the background flow is modulated on a length L and, specifically, consider the sinusoidal flow given by (2.7). In this case our previous solution yields what is simply an inner solution, valid on scales $r \ll L$. (Note that in the case of Poiseuille flow (2.6) G_b is zero, whereas now, in the full problem with the sinusoidal flow (2.7) or some other general background flow (2.2), G_b may be non-zero. It may be checked that G_b is negligible in the inner problem (5.1) with

† It should be noted that since ζ is exponentially small in the annular hole surrounding the vortex core, the coupling term (6.3) is potentially as important in equation (5.4*a*) as the other terms. Thus the expression for ζ in the region $1 \ll w \ll R^{1/3}$ is different from that given in M85. However the important outer solution (6.5) is essentially fixed by the far-field boundary condition within (6.1) and is independent of the detailed structure of ζ within $w \ll R^{1/3}$. The upshot is that although the presence of the stream coupling term has an O(1) *relative* effect on ζ within the hole, this quantity remains exponentially small there and does not influence the large-R result (6.8).

the scalings (2.8*a–c*) in force.) Our procedure now is to develop a straightforward expansion for the outer problem, which requires us to describe the evolution of vorticity on a scale $r = O(L)$. We impose the far-field boundary condition (4.4*b*) on this larger scale flow, match to complete the solution and thereby determine the vortex motion. In general this outer flow can be expected to involve all harmonics n, but only the $n = 1$ component will be relevant when the matching is performed.

Although our focus will be on $r = O(L)$ there is actually no need to formally rescale the problem. At a given time t the vortex has a scale of order $\sqrt{\nu t}$ and the 'hole' in the background is of size $\sqrt{R\nu t}$, or equivalently $\sqrt{\Gamma t}$. These scales are much less than L under the restrictions (2.8*a*) and (2.8*c*) that were placed on the analysis at the outset. For $r = O(L)$ the Gaussian vortex appears as a point vortex and background vorticity evolves as a passive scalar. We can therefore justifiably solve (4.2) with $\beta \simeq 0$ and $\alpha \simeq \Gamma/2\pi r^2 = R\nu r^{-2}$ (both correct to exponential accuracy). It is not necessary to obtain a solution for general times t and a power series expansion in time is quite sufficient in view of the restriction (2.8*c*). In addition, the leading-order correction is adequate for our needs, so we set

$$\omega(\boldsymbol{r}, t) = \Omega_{\mathrm{b}}(r, \theta) + \tilde{\omega}(r, \theta, t) + O(t^2), \tag{7.1a}$$

$$\psi(\boldsymbol{r}, t) = \Psi_{\mathrm{b}}(r, \theta) + \tilde{\psi}(r, \theta, t) + O(t^2) \tag{7.1b}$$

(recall (4.4*a*)), where

$$\partial_t \tilde{\omega} + \alpha(r)\partial_\theta \Omega_{\mathrm{b}} = \partial_t \tilde{\omega} + R\nu r^{-2}\partial_\theta \Omega_{\mathrm{b}} = 0 \tag{7.2}$$

gives immediately

$$\tilde{\omega} = -R\nu t r^{-2}\partial_\theta \Omega_{\mathrm{b}}. \tag{7.3}$$

Note that for the beta-plane problem in LS97, (7.2) is replaced by the equation for Rossby waves in the far field, as discussed in Appendix A.

For the particular background (2.7) this becomes

$$\tilde{\omega}(\boldsymbol{r}, t) = -2LR\mu\nu t r^{-2}\,\partial_\theta \sin(rL^{-1}\cos\theta) \tag{7.4}$$

and we are only really interested in the $n = 1$ component. With

$$\tilde{\omega} = \sum_n \tilde{\omega}_n(r, t)\exp(\mathrm{i}n\theta),$$

results given in chapter 9 of Abramowitz & Stegun (1965) show that

$$\tilde{\omega}_1(r, t) = -2\mathrm{i}LR\mu\nu t r^{-2} J_1(r/L). \tag{7.5}$$

This expression is valid for $r = O(L)$; in an overlap region with $r \ll L$, it reduces to

$$\tilde{\omega}_1(r, t) = -\mathrm{i}R\mu\nu t r^{-1} + \cdots \tag{7.6}$$

(see (7.8) below). Comparison with (5.13*a*) reveals that (7.6) is precisely the second term of the large-w form of the inner similarity solution, as indeed it ought to be. The first term in (5.13*a*) corresponds to the background Ω_{b} itself.

However, we really need the $n = 1$ mode of the stream function, $\tilde{\psi}_1$. This may be written in terms of $\tilde{\omega}_1$ given in (7.5) by inverting $-\tilde{\omega}_1 = \Delta_1 \tilde{\psi}_1$,

$$2\tilde{\psi}_1(r, t) = -r^{-1}\int_r^\infty \rho^2 \tilde{\omega}_1(\rho, t)\,\mathrm{d}\rho + r\int_r^\infty \tilde{\omega}_1(\rho, t)\,\mathrm{d}\rho + D_1 r^{-1} + E_1 r, \tag{7.7}$$

where D_1 and E_1 are arbitrary constants. To proceed, we note the standard properties of Bessel functions,

$$J_1(z) \sim \tfrac{1}{2}z \quad (z \to 0), \qquad J_1(z) \sim (2/\pi z)^{1/2} \cos\left(z - \tfrac{3}{4}\pi\right) \quad (z \to \infty) \tag{7.8}$$

and consider the limit $r \to \infty$. The two terms involving integrals give rise to contributions of order $r^{-3/2}$ to $\tilde{\psi}_1$ and so to comply with the far-field condition (5.2*b*) we must set $E_1 = 0$. Now, at last, we have been able to impose the proper far-field behaviour on the outer solution at scale $r \gg L$.

We need to ensure that (7.7) matches correctly onto the inner solution and this requires the behaviour of $\tilde{\psi}_1$ for small $r/L = z$, say. As $z \to 0$ so

$$\int_z^\infty z^{-2} J_1(z)\,\mathrm{d}z = -\tfrac{1}{2}\log z + c_1 + O(z^2), \qquad c_1 \equiv \tfrac{1}{2}\log 2 + \tfrac{1}{4} - \tfrac{1}{2}\gamma \simeq 0.307966. \tag{7.9}$$

The substitution of both (7.8) and (7.9) into (7.7) gives the behaviour of $\tilde{\psi}_1$ for small r as

$$\tilde{\psi}_1 = -\mathrm{i}R\mu\nu tr\left(-\tfrac{1}{2}\log(r/L) + C_1\right) + D_2 r^{-1}, \qquad C_1 \equiv c_1 + \tfrac{1}{4} = \tfrac{1}{2}(\log 2 + 1 - \gamma), \tag{7.10}$$

where D_2 is another constant that is of no interest here. This approximate form of the stream function of the outer expansion, valid as we approach the inner region, should match with the second term in (5.13*b*). This can be achieved by fixing $\dot{Z}^*$ appropriately, which gives the vortex velocity as

$$\dot{Z} = -R\mu\nu t\left[\tfrac{1}{2}\log(\nu t/L^2) - 2C_1 - 2\mathrm{i}F^*(R)\right] \tag{7.11}$$

and integration yields its position as

$$Z = -\tfrac{1}{2}R\mu\nu t^2\left(\tfrac{1}{2}\log(\nu t/L^2) - 2C_1 - 2\mathrm{i}F^*(R) - \tfrac{1}{4}\right), \tag{7.12}$$

taking $Z \to 0$ as $t \to 0^+$. It is convenient to rewrite this as

$$Z = -\tfrac{1}{2}R\mu\nu t^2\left(\tfrac{1}{2}\log(R\nu t/4L^2) + G(R)\right), \tag{7.13}$$

where, from (7.10),

$$G(R) = -\tfrac{1}{2}\log R - \tfrac{5}{4} + \gamma - 2\mathrm{i}F^*(R). \tag{7.14}$$

This theory is correct for any $R \geqslant O(1)$; in § 6 we computed $F(R)$ numerically for moderate values of R and the corresponding values of $G(R)$ are also listed in table 1 above. For $R \gg 1$ the asymptotic formula (6.2) gives $F(R)$ and implies that $G(R)$ is constant at this order of approximation

$$G(R) \simeq -\tfrac{5}{4} + \tfrac{3}{2}\gamma - \tfrac{1}{4}\mathrm{i}\pi \approx -0.3842 - \mathrm{i}0.7854; \tag{7.15}$$

so, for large R,

$$Z = -\tfrac{1}{2}R\mu\nu t^2\left[\tfrac{1}{2}\log(R\nu t/4L^2) - \tfrac{5}{4} + \tfrac{3}{2}\gamma - \tfrac{1}{4}\mathrm{i}\pi\right]. \tag{7.16}$$

Finally, replacing $R\nu = \Gamma/2\pi$ gives the high-R prediction for the movement of a vortex in a weak background; see equation (3.3). It should be remembered that this asymptotic form is in reasonable accord with the numerical simulations that were presented in § 3.

8. Point-vortex motion within an inviscid background

The relatively straightforward formula (3.3) for the motion of a vortex at large Reynolds number R suggests that the problem may be formulated in a completely

inviscid setting. Here we sketch the problem of the motion of a point vortex at $(X(t), Y(t))$ in a weak inviscid background vorticity distribution, given by $(\omega_b(x, y, t), \psi_b(x, y, t))$, and show how this reduces to the result (3.3). The exact nonlinear equations are (Schecter & Dubin 2001)

$$\partial_t \omega_b + J(\omega_b, \psi_b + \psi_v) = 0, \qquad \omega_b = -\nabla^2 \psi_b \tag{8.1}$$

for the background, and

$$\dot{X}(t) = \partial_y \psi_b(X(t), Y(t), t), \qquad \dot{Y}(t) = -\partial_x \psi_b(X(t), Y(t), t) \tag{8.2}$$

for the point vortex, with

$$\psi_v(x, y, t) = -(\Gamma/4\pi) \log[(x - X(t))^2 + (y - Y(t))^2]. \tag{8.3}$$

The appropriate initial conditions are that $\omega_b = \Omega_b$ at $t = 0$, and we must have $\psi_b = \Psi_b + O(r^{-1})$ for large r; for the remainder of this calculation we concentrate on the sinusoidal background (2.7).

The solution relating to a weak background flow may be determined by iteration, and only one step is required. The starting point is to assume that the vortex is fixed at the origin: this causes the background to wind up and we may compute the correction that gives rise to vortex motion. Notice that at large, but finite, Reynolds number the hole in the background vorticity grows as $\sqrt{\Gamma t}$ while the vortex position is proportional to μt^2 plus logarithmic corrections. Thus this is a consistent procedure for large R as the vortex always remains inside the hole for moderate times; even for infinite R the procedure makes sense on the basis that the dominant contribution to the vortex motion from the background arises at distances of order $\sqrt{\Gamma t}$ from the vortex.

Within this framework the action of the fixed vortex on the background gives

$$\partial_t \omega_b + (\Gamma/2\pi r^2) \partial_\theta \omega_b = 0 \tag{8.4}$$

and if ω_b and ψ_b are broken into Fourier harmonics ω_n and ψ_n, knowledge of ψ_1 is sufficient to compute the leading effect of vortex motion. For the initial background (2.7) it follows that

$$\omega_1(r, t) = 2L\mu J_1(r/L) \exp(-\mathrm{i}\Gamma t/2\pi r^2); \tag{8.5}$$

we need then to retrieve ψ_1 and hence evaluate the vortex velocity defined by

$$\dot{Z} = -2\mathrm{i}(\partial_r \psi_1)^*|_{r=0}. \tag{8.6}$$

In general

$$2\psi_1(r, t) = r^{-1} \int_0^r \rho^2 \omega_1(\rho, t)\, \mathrm{d}\rho + r \int_r^\infty \omega_1(\rho, t)\, \mathrm{d}\rho + D_1 r^{-1} + E_1 r \tag{8.7}$$

which can be rewritten as

$$\xi_1(s, t) = s^{-1} \int_0^s \sigma^2 J_1(\sigma) \mathrm{e}^{-\mathrm{i}Q/\sigma^2}\, \mathrm{d}\sigma + s \int_s^\infty J_1(\sigma) \mathrm{e}^{-\mathrm{i}Q/\sigma^2}\, \mathrm{d}\sigma + D_2 s^{-1} + E_2 s, \tag{8.8}$$

where

$$\xi_1(s, t) \equiv \psi_1(r, t)/\mu L^3, \qquad s = r/L, \qquad Q = \Gamma t/2\pi L^2 \ll 1. \tag{8.9}$$

For $Q = 0$, i.e. $t = 0$, in (8.8), these equations link

$$\omega_1 = 2\mu L J_1(r/L), \qquad \psi_1 = 2\mu L^3 (J_1(r/L) - r/2L) \tag{8.10}$$

(corresponding to (2.7)) with

$$D_2 = 0, \qquad E_2 = -1, \tag{8.11}$$

whereupon (8.6) shows that $\dot{Z} = 0$, as would be anticipated at $t = 0$.

It may be verified that the constants D_2 and E_2 continue to be given by (8.11) for a general value of t; this ensures the correct far field is $\psi_b = \Psi_b + O(r^{-1})$ for large r. Given this, we now consider

$$\begin{aligned}\tilde{\xi}_1(s,t) &\equiv \xi_1(s,t) - \xi_1(s,0) \\ &= s^{-1}\int_0^s \sigma^2 J_1(\sigma)\left(e^{-iQ/\sigma^2} - 1\right) d\sigma + s\int_s^\infty J_1(\sigma)\left(e^{-iQ/\sigma^2} - 1\right) d\sigma\end{aligned} \tag{8.12}$$

and wish to evaluate

$$\dot{Z} = -2i\mu L^2 (\partial_s \tilde{\xi}_1)^*|_{s=0}, \tag{8.13}$$

from (8.6). Differentiating (8.12) gives

$$\partial_s \tilde{\xi}_1|_{s=0} = \int_0^\infty J_1(\sigma)\left(e^{-iQ/\sigma^2} - 1\right) d\sigma \tag{8.14}$$

and we require this integral to leading order in Q for small Q; recall that Q is proportional to t by (8.9). To compute this integral we break up the range by introducing a parameter Σ with $\sqrt{Q} \ll \Sigma \ll 1$. Throughout $0 \leqslant \sigma \leqslant \Sigma$ the Bessel function component may be expanded in powers of σ giving rise to exponential integrals (6.7), while for $\Sigma \leqslant \sigma$ the exponential may be written in powers of Q/σ^2, leading to integrals such as (7.9). We omit the details, which clearly now parallel our earlier calculations, and result in

$$\partial_s \tilde{\xi}_1|_{s=0} = \tfrac{1}{2} iQ\left(\tfrac{1}{2}\log Q + \tfrac{3}{2}\gamma - \log 2 - 1 + \tfrac{1}{4}i\pi\right) + O(Q^2). \tag{8.15}$$

This calculation then recovers $\dot{Z}$ as given in (7.11). Note that while this calculation gives the inviscid result quite quickly, it does not reveal much about the structure of the vorticity field in the presence of viscosity, for example the hole around the vortex seen in figure 2.

9. Further numerical comparison and discussion

To close our work we present some further numerical results, and study them in more detail than figure 3; our aim is to investigate to what extent they support the theory we have developed. Also we should be wary that the theory involved placing a point vortex in an incompressible fluid at $t = 0$, and so involves a logarithmic divergence in the vortex acceleration as $t \to 0$: it is important to check that our results are robust to the case of a finite initial vortex as simulated numerically.

We rewrite (7.13) in a simpler form by introducing a rescaled vortex displacement $Z' = X' + iY'$ and rescaled time t' given by

$$Z'/Z = R\nu/16\mu L^4, \qquad t'/t = R\nu/4L^2, \tag{9.1}$$

whereupon

$$Z' = X' + iY' = -\tfrac{1}{2}t'^2\left[\tfrac{1}{2}\log t' + G(R)\right] \tag{9.2}$$

for any R and, in particular, for large R,

$$Z' = X' + iY' = -\tfrac{1}{2}t'^2\left[\tfrac{1}{2}\log t' - \tfrac{5}{4} + \tfrac{3}{2}\gamma - \tfrac{1}{4}i\pi\right]. \tag{9.3}$$

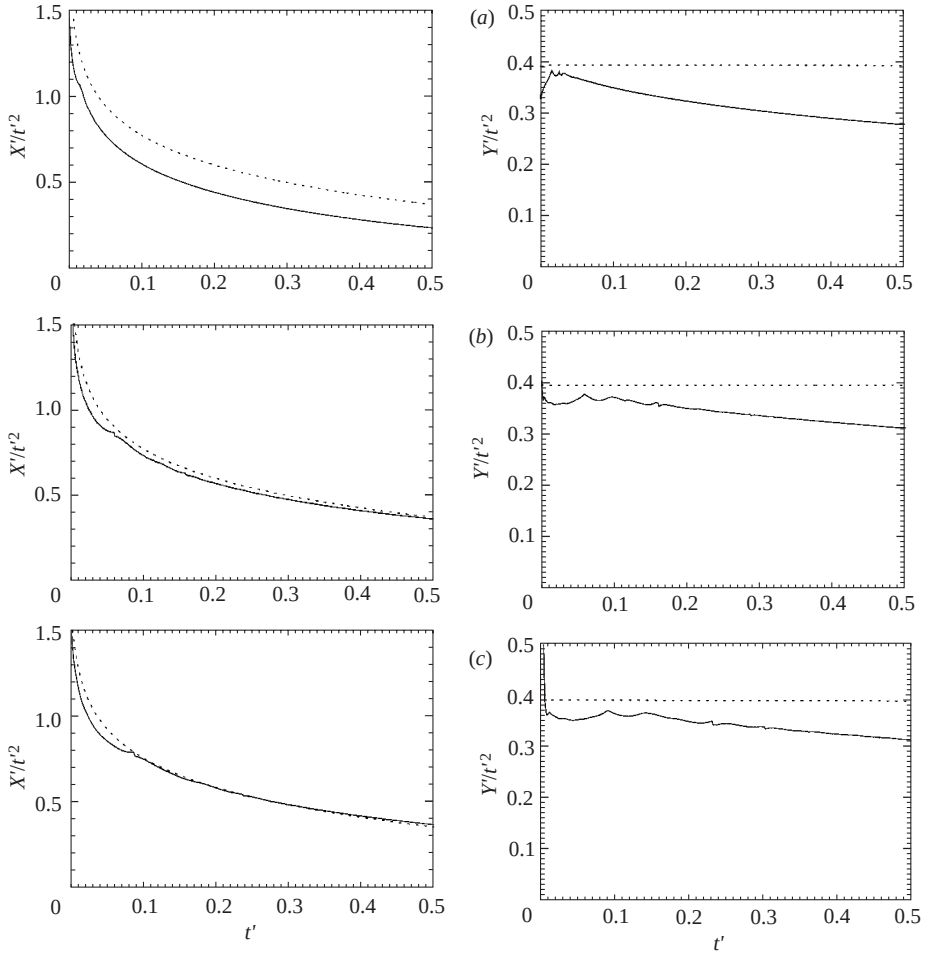

FIGURE 4. Plots of X'/t'^2 (left panels) and Y'/t'^2 (right panels) against t', for (*a*) $L=1$, $\mu=0.75$; (*b*) $L=\frac{1}{2}$, $\mu=2$; and (*c*) $L=\frac{1}{3}$, $\mu=5$. Shown are numerical results (solid) compared with the asymptotic theory for large R (dotted).

Figure 4 shows a series of runs with X'/t'^2 (left panels) and Y'/t'^2 (right panels) plotted. Initially let us concentrate on the top pair of panels which corresponds to the choices $L=1$, $\mu=0.75$, $\Gamma=2\pi$, $\nu=0.001$ and so $R=1000$; this run is therefore practically inviscid and suggests that the formula (9.3) is applicable. The calculation was performed using a resolution of 1024^2 and an initial vortex radius of $r_0=0.005$. There are clearly some discrepancies between the numerical (solid) and asymptotic (dotted) findings. Most noticeably the form of X'/t'^2 shows a fixed displacement between the two curves, suggesting that there is possibly a problem with the constants appearing in (9.3). In contrast, the curve for Y'/t'^2 tends to the correct level for small times, but then drifts away, presumably because higher-order (longer time) effects that were ignored in our analysis begin to come into play. Both curves exhibit initial 'glitches', whose importance is exaggerated by our dividing X' and Y' by t'^2. These glitches may be traced to the numerical compromises of the initial vortex being of finite, rather than zero, radius, and the fact that a finite grid is used. Indeed, close examination shows that there are also other very minor glitches in the curves in

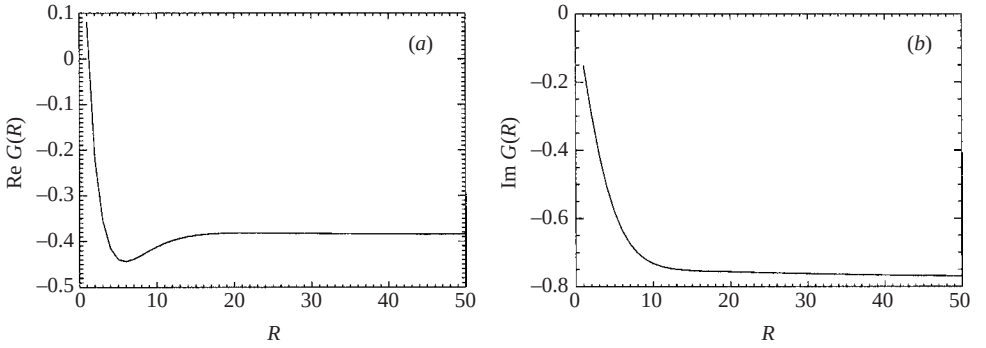

FIGURE 5. Plotted are (*a*) the real and (*b*) imaginary components of $G(R)$ as functions of the Reynolds number R.

figure 4; these arise due to the change of interpolation used to locate the vortex maximum as it crosses grid points in the simulation.

The issue of the constant displacement in X'/t'^2, corresponding to a query over our calculation of the X-motion, appears to be a consequence of our use of periodic boundary conditions. Our analytical study was developed for a single vortex within an infinite sinusoidal background vorticity distribution, whereas numerically we have taken periodic boundary conditions. At face value this might not seem too crucial but our workings have revealed that this difference might be important. We have seen (as in LS97) that the far field of the vorticity distribution plays an important role in fixing the logarithmic divergence and so determining the constants in (9.3). The far fields in the periodic numerical domain and the analytical, isolated vortex calculation are different!

To check this hypothesis we performed further simulations in the periodic geometry $[-\pi, \pi]^2$ but now with $L = \frac{1}{2}$ and $L = \frac{1}{3}$; the outcomes are shown in figure 4(*b*, *c*). In each case there is still just the single vortex in a periodicity box, but in the three cases illustrated in figure 4 we have one per 1, 2 and 3 wavelengths of the background respectively. Values for the vorticity gradient were taken to be $\mu = 2$ and 5 for the latter two cases. It is clear that the agreement with the theoretical results improves markedly as the numerical configuration approaches the analytical one of a single vortex in a sinusoidal background. This is especially the case for X'/t'^2; for Y'/t'^2 the agreement is less good, but still satisfactory. We conclude that our conjecture is correct and that the discrepancy between the theory and the computations has its origins in the difference between the analytical and numerical configurations. When this is accounted for, the numerical evidence gives good confirmation of our theory.

We have also undertaken a number of runs at lower Reynolds numbers down to $R = 10$ (not shown). Surprisingly, the results seem to be almost independent of R in this range, a result which may be attributed to the form of $G(R)$; see (7.14). This function, which captures the Reynolds number dependence of the motion, is constant within our approximations, and numerically varies rather slowly with R in this range, as may be seen from table 1, or graphically in figure 5. Above $R \simeq 10$, the effects of a finite Reynolds number are too small for us to distinguish within the limitations of our numerical simulations (in particular with our finite initial vortex size and the use of a periodic rather than infinite geometry). At Reynolds numbers much below about $R = 10$ the initial vortex diffuses outwards too quickly for us numerically to

obtain a good scale separation between the initial vortex extent and the scale of the background vorticity gradient.

These numerical results conclude our paper, in which we have studied the motion of a vortex in weak background vorticity. Our analytical approach has been founded on linearization about a strong vortex; this precludes the background vorticity having its own dynamical evolution (for example supporting waves that might travel away from the vicinity of the vortex). The findings highlight the role of logarithmic divergences, through which the vortex motion depends on the far field of the vorticity distribution. This was also evident numerically, in comparing the periodic geometry used for computational convenience, with the infinite geometry adopted for the analytical calculation. In fact we may now revisit the limit of a spatially infinite vorticity gradient by considering equation (7.16) and taking the limit $L \to \infty$. At any fixed time $t > 0$, the distance X travelled in the x-direction increases as $L \to \infty$; the average velocity of the vortex over any finite time interval increases as a result of summing contributions to the velocity from vorticity at increasing distances. This leads to the ill-posedness of the linearized problem in an infinite uniform vorticity gradient, as seen in the related beta-plane problem (LS97). Another striking feature is how insensitive our results are to Reynolds number above about $R = 10$.

Extensions of the present work to more general background flows would be of interest, and in Appendix B we give results relating to a more general unidirectional shear flow than the pure sinusoidal example considered here. As mentioned at the end of the introduction the problem of vortex motion on a beta-plane is a fundamental one in geophysical fluid dynamics. An interesting adaptation of our present study would be to include a beta-effect and so determine the interaction of motion induced by the variation of Coriolis parameter with latitude, and that driven by vorticity wind-up as studied here. Such an investigation may be relevant to understanding motion of geophysical vortices in the presence of jets or other shear flows.

We would like to thank Dr T. Lipniacki and Professor V. Shrira for helpful discussions and useful references. We are also grateful to anonymous referees for their insightful comments and for stressing the relationship of our work with LS97.

This work was supported by the British/Polish Joint Research Collaboration Programme of the British Council and the Komitet Badań Naukowych (KBN). A. G. would like to thank staff of the Institute of Geophysics of Warsaw University for their hospitality, and likewise K. B. the staff of the School of Mathematical Sciences of the University of Exeter. K. B. acknowledges further support from the KBN under grant number 2 P03B 13517.

Appendix A. The beta-effect and relation with LS97

In this appendix we sketch the relationship of our study with that of LS97, which should be studied for additional background and references. First let us incorporate the beta effect in our analysis, which we suppose has constant magnitude $\bar{\beta}$, giving in place of (2.1)

$$\partial_t \Omega + J(\Omega, \Psi) - \bar{\beta}\partial_x \Psi = 0, \qquad \Omega = -\nabla^2 \Psi. \tag{A 1}$$

We have also dropped the viscous and forcing terms. Our study has focused on the situation where the initial condition incorporates a vortex in a background shear flow (2.6) or (2.7). The comparison with LS97 is clearest if we subtract off this background

flow at the outset. Let us focus on (2.6) in the first instance and set

$$\Omega = 2\mu y + \Omega', \qquad \Psi = -\tfrac{1}{3}\mu y^3 + \Psi'; \tag{A 2}$$

here a prime is just a label and we have rotated the background flow through $\pi/2$.

We will take μ and $\bar{\beta}$ to be of similar size and with no length scale L yet introduced our discussion will be valid for

$$\Gamma t \ll L_{\rm vb}^2, \qquad L_{\rm vb} \equiv (\Gamma/\mu)^{1/3}, \tag{A 3}$$

from (2.8*b*, *c*). Note that in the beta-plane context, $L_{\rm vb}$ can be seen as a Rhines (1975) scale, where the phase velocity of Rossby waves (of order $\bar{\beta}L_{\rm vb}^2$) is similar to that of the fluid flow (of order $\Gamma/L_{\rm vb}$). Equation (A 1) becomes

$$\partial_t \Omega' + J(\Omega', \Psi') - (2\mu + \bar{\beta})\partial_x \Psi' - \mu y^2 \partial_x \Omega' = 0 \tag{A 4}$$

(with $\Omega' = -\nabla^2 \Psi'$), and we see that in the third term the background flow for $\mu \neq 0$ enters in precisely the same way as the beta-effect term. However, there is an additional, fourth term for $\mu \neq 0$, which represents the advection of vorticity by the background flow.

Now consider solving this inviscid problem with the initial condition of a point vortex at the origin (though LS97 discusses a more general initial axisymmetric vortex). In the inner problem with $r \ll L_{\rm vb}$, the leading-order balance is trivially satisfied between the first two terms of (A 4) for a point vortex $\Omega' = \Omega_{\rm v} = \Gamma\delta(x)\delta(y)$ and $\Psi' = \Psi_{\rm v} = -(\Gamma/2\pi)\log r$. At order μ (or $\bar{\beta}$) the third term generates a correction and we obtain

$$\Omega' = \Omega_{\rm v} + \left(\mu + \tfrac{1}{2}\bar{\beta}\right) {\rm i} r \left(1 - {\rm e}^{-{\rm i}\alpha(r)t}\right) {\rm e}^{{\rm i}\theta} + {\rm c.c.} + \cdots, \tag{A 5a}$$

$$\Psi' = \Psi_{\rm v} - \tfrac{1}{4}\left(\mu + \tfrac{1}{2}\bar{\beta}\right) {\rm i} r^3 \left(E_3(z) - E_2(z) + \tfrac{1}{2}\right) {\rm e}^{{\rm i}\theta} + A_1 r {\rm e}^{{\rm i}\theta} + {\rm c.c.} + \cdots, \tag{A 5b}$$

with $\alpha = \Gamma/2\pi r^2$ and $z = {\rm i}\Gamma t/2\pi r^2$. Thus the inner problems are identical in LS97 and in this paper (except that we include viscosity).

Note that when these expansions are substituted into (A 4) the first three terms are all of size $\mu\Gamma/r$. It may be checked that for $r \ll L_{\rm vb}$, in this solution the fourth term in (A 4) remains subdominant in the solution as found so far, being of size $\mu^2\Gamma t$. The ratio of the fourth term divided by the first is $\mu r t \sim (\Gamma t/L_{\rm vb}^2)(r/L_{\rm vb}) \ll 1$.

Now the far field of the inner problem is given by $\Gamma t \ll r^2 \ll L_{\rm vb}^2$, with

$$\Omega' = \Omega_{\rm v} - \left(\mu + \tfrac{1}{2}\bar{\beta}\right)(\Gamma t/2\pi r) {\rm e}^{{\rm i}\theta} + {\rm c.c.} + \cdots, \tag{A 6a}$$

$$\Psi' = \Psi_{\rm v} - \left(\mu + \tfrac{1}{2}\bar{\beta}\right)(\Gamma t r/8\pi)[\log(\Gamma t/2\pi r^2) + \gamma + {\rm i}\pi/2] {\rm e}^{{\rm i}\theta} + A_1 r {\rm e}^{{\rm i}\theta} + {\rm c.c.} + \cdots. \tag{A 6b}$$

Using this it is readily checked that the second, Jacobian term in (A 4) becomes subdominant. In fact while the first and third terms remain of order $\mu\Gamma/r$, the second one falls to $\mu\Gamma^2 t/r^3$ and so drops out as we enter the far field $r^2 \gg \Gamma t$.

Now to obtain the LS97 framework we just set $\mu = 0$ above, and we are left with simply the first and third terms in (A 4). This describes Rossby wave radiation and LS97 derives Green's functions for this, with the appropriate causal properties (radiation propagating outwards), and then matches to fix A_1. The natural scale of this radiation process is given by $\bar{\beta} r t = O(1)$.

For our situation we set $\bar{\beta} = 0$, in which case we again have the first and third terms in (A 4), but the fourth term may also become important. In the far field of the inner solution, the first and third terms remain of order $\mu\Gamma/r$, while the fourth is again of order $\mu^2\Gamma t$. The first, third and fourth become comparable at a scale $\mu r t = O(1)$. If all these terms are retained, we are studying the motion of a vortex in a shear flow

that becomes strong at large distances, as done by Schecter & Dubin (2001). In this case the fourth term, advection of vorticity by the background, becomes comparable to the third at a scale $r = O(L_{\rm vb}^3/\Gamma t)$ as might be expected, and one would need to match to the behaviour at this scale.

We have however not followed this route, but have instead modulated the background shear on a large length scale L. This leads to replacing (2.6) by (2.7) and so (A 4) by

$$\partial_t \Omega' + J(\Omega', \Psi') - (2\mu\cos(y/L) + \bar{\beta})\partial_x \Psi' - 2\mu L^2(1 - \cos(y/L))\partial_x \Omega' = 0. \quad \text{(A 7)}$$

We now take the inequalities (2.8b, c) to hold. Here the third term remains of its previous magnitude, but while the fourth term remains of size $\mu^2\Gamma t$ for $r \ll L$, it decays as $\mu^2\Gamma t L^2/r^2$ for $r \gg L$. So now the fourth term is small in comparison with the first in all of space, the ratio being $(\Gamma t/L_{\rm vb}^2)(L/L_{\rm vb})(L/r) \ll 1$ for $r \gg L$.

This confirms our analysis, in which the fourth, vorticity advection term did not play a role in the regularization of our logarithmic divergence at scale L. It also indicates that the problem of vortex motion in the presence of a beta effect as well as a shear flow modulated on a scale L is sensibly addressed within the framework of LS97 and this paper, with $\bar{\beta}$ and μ of similar magnitude and inequalities (2.8) holding. In this case it would be necessary to develop LS97 by using the Green's function for Rossby wave radiation. In Laplace-transform space, deleting the subdominant fourth and second terms, this would amount to solving (using obvious notation)

$$p\bar{\Omega}' - (2\mu\cos(y/L) + \bar{\beta})\partial_x \bar{\Psi}' = 0. \quad \text{(A 8)}$$

The tractability of this approach and the scope for obtaining geophysically informative results, remain subjects for further investigation.

Appendix B. Vortex motion in a general unidirectional shear flow

Consider the vorticity distribution and fluid flow

$$\Omega_{\rm b} = \sum_{n=1}^{\infty} \Omega_n \sin(nx/L), \qquad \boldsymbol{U}_{\rm b} = \sum_{n=0}^{\infty} U_n \cos(nx/L)\,\hat{\boldsymbol{y}}, \quad \text{(B 1)}$$

with $\Omega_n = -nU_n/L$ and U_0 fixed so that the fluid particle at the origin is at rest. The vorticity gradient at the origin is then given by

$$2\mu = \sum_{n=1}^{\infty} n\Omega_n/L. \quad \text{(B 2)}$$

There is no need for cosine terms in $\Omega_{\rm b}$ or sine terms in $\boldsymbol{U}_{\rm b}$; by symmetry these cannot give rise to vortex motion. We also assume that the terms Ω_n decrease rapidly with increasing n in order to maintain a clear scale separation between the background vorticity distribution and the vortex itself.

The inner solution proceeds exactly as before with this value of μ up to equations (5.13). For the outer solution we follow § 7 to obtain in place of (7.5),

$$\tilde{\omega}_1(r, t) = -\mathrm{i}Rvtr^{-2} \sum_{n=1}^{\infty} \Omega_n J_1(nr/L), \quad \text{(B 3)}$$

and expression (7.7) for the stream function gives

$$\tilde{\psi}_1 = -\mathrm{i}Rvtr \sum_{n=1}^{\infty} \tfrac{1}{2} n\Omega_n L^{-1}\left(-\tfrac{1}{2}\log(nr/L) + C_1\right) + D_2 r^{-1}, \quad \text{(B 4)}$$

analogous to (7.10). This may be rewritten as

$$\tilde{\psi}_1 = -\mathrm{i}R\mu\nu tr\left(-\tfrac{1}{2}\log(r/L_*) + C_1\right) + D_2 r^{-1}, \tag{B 5}$$

where L_* is given by a weighted geometric mean,

$$L_* = \prod_{n=1}^{\infty}(L/n)^{w_n}, \qquad w_n \equiv n\Omega_n/2\mu L. \tag{B 6}$$

The calculation then proceeds to yield equations for $\dot{Z}$ and Z that are identical to those in §§6–8, save that the scale L needs to be replaced by L_*.

REFERENCES

Abramowitz, M. & Stegun, I. A. 1965 *Handbook of Mathematical Functions*. Dover.

Bajer, K. 1998 Flux expulsion by a point vortex. *Eur. J. Mech.* B/*Fluids* **17**, 653–664.

Bajer, K., Bassom, A. P. & Gilbert, A. D. 2001 Accelerated diffusion in the centre of a vortex. *J. Fluid Mech.* **437**, 395–411.

Balmforth, N. J., del Castillo Negrete, D. & Young, W. R. 1997 Dynamics of vorticity defects in shear. *J. Fluid Mech.* **333**, 197–230.

Balmforth, N. J., Llewellyn Smith, S. G. & Young, W. R. 2001 Disturbing vortices. *J. Fluid Mech.* **426**, 95–133.

Bassom, A. P. & Gilbert, A. D. 1998 The spiral wind-up of vorticity in an inviscid planar vortex. *J. Fluid Mech.* **371**, 109–140.

Bassom, A. P. & Gilbert, A. D. 1999 The spiral wind-up and dissipation of vorticity and a passive scalar in a strained planar vortex. *J. Fluid Mech.* **398**, 245–270.

Bassom, A. P. & Gilbert, A. D. 2000 The relaxation of vorticity fluctuations in approximately elliptical stream lines. *Proc. R. Soc. Lond.* A **456**, 295–314.

Bernoff, A. J. & Lingevitch, J. F. 1994 Rapid relaxation of an axisymmetric vortex. *Phys. Fluids* **6**, 3717–3723.

Brachet, M. E., Meneguzzi, M., Politano, H. & Sulem, P.-L. 1988 The dynamics of freely decaying two-dimensional turbulence. *J. Fluid Mech.* **194**, 333–349.

Briggs, R. J., Daugherty, J. D. & Levy, R. H. 1970 Role of Landau damping in crossed-field electron beams and inviscid shear flow. *Phys. Fluids* **13**, 421–432.

Brunet, G. & Montgomery, M. T. 2002 Vortex Rossby waves on smooth circular vortices. Part I. Theory. *Dyn. Atmos. Oceans* **35**, 153–177.

Cushman-Roisin, B. 1994 *Introduction to Geophysical Fluid Dynamics*. Prentice Hall.

Dritschel, D. G. 1989 Contour dynamics and contour surgery: numerical algorithms for extended high-resolution modelling of vortex dynamics in two-dimensional, inviscid, incompressible flows. *Comput. Phys. Rep.* **10**, 77–146.

Fornberg, B. 1977 A numerical study of 2-d turbulence. *J. Comput. Phys.* **25**, 1–31.

Gilbert, A. D. 1988 Spiral structures and spectra in two-dimensional turbulence. *J. Fluid Mech.* **193**, 475–497.

Hall, I. M., Bassom, A. P. & Gilbert, A. D. 2003*a* The effect of fine structure on the stability of planar vortices. *Eur. J. Mech.* B/*Fluids* **22**, 179–198.

Hall, I. M., Bassom, A. P. & Gilbert, A. D. 2003*b* The effect of viscosity on the stability of planar vortices with fine structure. *Q. J. Mech. Appl Maths* **56**, 649–657.

Le Dizès, S. 2000 Non-axisymmetric vortices in two-dimensional flows. *J. Fluid Mech.* **406**, 175–198.

Lingevitch, J. F. & Bernoff, A. J. 1995 Distortion and evolution of a localized vortex in an irrotational flow. *Phys. Fluids* **7**, 1015–1026.

Llewellyn Smith, S. G. 1995 The influence of circulation on the stability of vortices to mode-one disturbances. *Proc. R. Soc. Lond.* A **451**, 747–755.

Llewellyn Smith, S. G. 1997 The motion of a non-isolated vortex on the beta-plane. *J. Fluid Mech.* **346**, 149–179 (referred to herein as LS97).

Lundgren, T. S. 1982 Strained spiral vortex model for turbulent fine structure. *Phys. Fluids* **25**, 2193–2203.

Macaskill, C., Bassom, A. P. & Gilbert, A. D. 2002 Nonlinear wind-up in a strained planar vortex. *Eur. J. Mech.* B/*Fluids* **21**, 293–306.

McCalpin, J. D. 1987 On the adjustment of azimuthally perturbed vortices. *J. Geophys. Res.* C **92**, 8213–8225.

McWilliams, J. C. 1984 The emergence of isolated coherent vortices in turbulent flow. *J. Fluid Mech.* **146**, 21–43.

Moffatt, H. K. & Kamkar, H. 1983 On the time-scale associated with flux expulsion. In *Stellar and Planetary Magnetism* (ed. A. M. Soward), pp. 91–97. Gordon & Breach.

Montgomery, M. T. & Brunet, G. 2002 Vortex Rossby waves on smooth circular vortices. Part II. Idealized numerical experiments for tropical cyclone and polar vortex interiors. *Dyn. Atmos. Oceans* **35**, 179–204.

Moore, D. W. 1985 The interaction of a diffusing line vortex and an aligned shear flow. *Proc. R. Soc. Lond.* A **399**, 367–375 (referred to herein as M85).

Pearson, C. F. & Abernathy, F. H. 1984 Evolution of the flow field associated with a streamwise diffusing vortex. *J. Fluid Mech.* **146**, 271–283.

Reznik, G. M. & Dewar, W. K. 1994 An analytical theory of distributed axisymmetric barotropic vortices on the beta-plane. *J. Fluid Mech.* **269**, 301–321.

Rhines, P. B. 1975 Waves and turbulence on a beta-plane. *J. Fluid Mech.* **69**, 417–443.

Rhines, P. B. & Young, W. R. 1982 Homogenization of potential vorticity in planetary gyres. *J. Fluid Mech.* **122**, 347–367.

Rhines, P. B. & Young, W. R. 1983 How rapidly is a passive scalar mixed within closed streamlines? *J. Fluid Mech.* **133**, 133–145.

Schecter, D. A. & Dubin, D. H. E. 1999 Vortex motion driven by a background vorticity gradient. *Phys. Rev. Lett.* **83**, 2191–2194.

Schecter, D. A. & Dubin, D. H. E. 2001 Theory and simulations of two-dimensional vortex motion driven by a background vorticity gradient. *Phys. Fluids* **13**, 1704–1723.

Schecter, D. A., Dubin, D. H. E., Cass, A. C., Driscoll, C. F., Lansky, I. M. & O'Neil, T. M. 2000 Inviscid damping of asymmetries on a 2-d vortex. *Phys. Fluids* **12**, 2397–2412.

Smith, G. B. & Montgomery, M. T. 1995 Vortex axisymmetrization: dependence on azimuthal wave-number or asymmetric radial structure changes. *Q. J. R. Met. Soc.* **121**, 1615–1650.

Smith, R. A. & Rosenbluth, M. N. 1990 Algebraic instability of hollow electron columns and cylindrical vortices. *Phys. Rev. Lett.* **64**, 649–652.

Sutyrin, G. G. 1989 Azimuthal waves and symmetrization of an intense vortex. *Sov. Phys. Dokl.* **34**, 104–106.

Sutyrin, G. G. & Morel, Y. G. 1997 Intense vortex motion in a stratified fluid on the beta-plane: an analytical theory and its validation. *J. Fluid Mech.* **336**, 203–220.

Ting, L. & Klein, R. 1991 *Viscous Vortical Flows.* Lecture Notes in Physics, vol. 374. Springer.

Vassilicos, J. C. 1995 Anomalous diffusion of isolated flow singularities and of fractal or spiral structures. *Phys. Rev.* E **52**, R5753–R5756.